

The excellent gas barrier properties and unique mechanical properties of poly(propylene carbonate)/organo-montmorillonite nanocomposites

Junjun Kong^{1,2} · Zonglin Li^{1,2} · Zenwen Cao^{1,3} ·
Changyu Han¹ · Lisong Dong¹

Received: 16 January 2017 / Revised: 22 March 2017 / Accepted: 25 March 2017 /
Published online: 29 March 2017
© Springer-Verlag Berlin Heidelberg 2017

Abstract Intercalated nanocomposites comprised of poly(propylene carbonate) (PPC) and organo-montmorillonite (OMMT) were prepared via a direct melt blending method. The morphological, thermal, rheological, mechanical, and gas barrier properties of composites were carried out in detail. Results of XRD, TEM, and SEM revealed that OMMT dispersed homogeneously in the polymer matrix, and were intercalated by PPC macromolecules. Compared with neat PPC, the PPC/OMMT nanocomposites showed an enhancement in the 5 wt% weight loss temperature ($T_{-5\%}$) by near 20 °C with 3 phr OMMT concentration. With the percolation threshold formed, the rheological properties of composites translated from a liquid-like behavior to a solid-like one. Interestingly, PPC/OMMT nanocomposites revealed a concurrent improvement in the modulus, yield strength, and toughness with the addition of homogeneously dispersed clay. The oxygen permeability of well-dispersed PPC/OMMT nanocomposites reduced significantly compared with that of neat PPC. Consequently, this convenient and effective method, which facilitates to prepare PPC/OMMT nanocomposites with superior mechanical properties and excellent gas barrier performances, can be considered to broaden the application of PPC.

✉ Changyu Han
cyhan@ciac.ac.cn

✉ Lisong Dong
dongls@ciac.ac.cn

¹ Key Laboratory of Polymer Ecomaterials, Changchun Institute of Applied Chemistry, Chinese Academy of Sciences, 5625 Renmin Street, Changchun 130022, People's Republic of China

² University of Chinese Academy of Science, Beijing 10080, People's Republic of China

³ University of Science and Technology of China, Hefei 230027, Anhui, People's Republic of China

Keywords Poly(propylene carbonate) · Nanocomposites · Mechanical properties · Gas barrier

Introduction

Polymers are emerging materials with functionality, lightweight, ease processing, and low cost. They have an opportunity to replace many conventional materials (e.g., metals, ceramic and paper) in the packaging and other application fields [1]. Poly(propylene carbonate) (PPC) with decent biocompatibility and biodegradability has attracted increasing interest in last two decades. PPC is manufactured by the “alternating” copolymerization of epoxy compound and carbon dioxide which is proposed by Inoue et al. at the end of the 1960s for the first time [2]. The consumption of CO₂ in the production process of this kind of polyester can not only reduce the pollution of carbon dioxide but also contribute to resolving the shortage of petroleum. The biodegradability of PPC is beneficial to relieve the “white pollution” problem as well [3–5]. Generally speaking, the amorphous polymer PPC has superior characteristics of tensile toughness, transparency, and relative great gas barrier properties. However, using PPC separately in practical applications is limited by its glass transition temperature. Meanwhile, the inferior tensile strength of PPC goes against a wide range of its application [6]. Blending PPC with other polymers can enlarge its applications. Nevertheless, most polymers with high processing temperature are not suitable for compositing with PPC, since PPC begins to degrade at around 180 °C. Therefore, improving the thermal stability of PPC is necessary for broadening its application [3, 6–9].

Both in industry and academia, polymer nanocomposites containing montmorillonite layer silicates (MMT) have attracted great interests because of their high mechanical properties, superior thermal stability, excellent gas barrier performances, and outstanding biodegradability [10–13]. The 2:1 phyllosilicates montmorillonite with a high aspect ratio is considered impermeability for gas molecules. Thus, the dispersed nanoplatelets can inhibit the transmission of gases and make contributions to the gas barrier properties to the polymer nanocomposites. It is reported that with addition of small amount of nanoclays can reduce gas permeability through polymer films for about 50–500 times [14]. Moreover, the exchangeable cations adsorbed on the silicate layer make it possible to change from hydrophilic to organophilic. It is well known that the properties of nanocomposites are mainly determined by the dispersion of clay nanoplatelets in polymers and the interaction between nanofillers and matrix. The more homogeneously nanoplatelets disperse in polymer matrix, the more superior properties will be acquired, such as the well-dispersed and randomly exfoliated Polylactide (PLA)/MMT composites prepared by Du et al. [15] through melt blending. Their results showed that the randomly exfoliated montmorillonite particles decreased the diffusion coefficient of water vapor in composites by effectively increasing tortuosity of the pathway for water molecules to pass through the polymer membrane. Ion exchange reactions have been used by modifying the layered silicates to make OMMT compatible with non-polar polymers to achieve a well-dispersed nanocomposite. Converting the hydrophilic silicate surface into organophilic can improve the dispersion of MMT in

polymer matrix. Richert et al. [16] discussed the influence of two types of MMT (Cloisite 30B and Nanofil 2) on transmission rates of water vapor, oxygen, and carbon dioxide for PLA nanocomposites. They found that the hydrophobic Cloisite 30B decreased the gas permeability much more effectively than the hydrophilic Nanofil 2. At the same time, the compatible nanocomposites reduced the carbon dioxide transmission rate more significantly. Various methods such as in situ polymerization [17–19], solution [20, 21], and latex methods [22] are used to form homogeneously dispersed nanocomposites. Melt blending is the most convenient, low cost, and high yield technique to prepare polymer nanocomposites. Khan et al. [23] and Xu et al. [24] had produced partially exfoliated PPC/clay nanocomposites through melt blending, and this nanocomposite showed higher elastic modulus, hardness, and anti-water absorption capacity than those of pure PPC. However, polymer nanocomposites make contributions to enhancement in stiffness and strength also at the expense of ductile. Even with so many advantages, melt blending is reported to give rise to the thermal degradation of PPC inevitably during the melt compounding process [25].

In this paper, we reported a direct melt intercalation of PPC/organo-montmorillonite (OMMT) nanocomposites and gave a detailed explanation about the transformation of thermal and rheological characteristic of the nanocomposites. Moreover, the research mainly focused on further enhancing the mechanical and gas barrier properties of PPC/OMMT nanocomposites. The novelty of the work is the concurrent improvement in the modulus, yield strength, and toughness with the addition of OMMT. As far as we know, this is the first report about the gas barrier properties of PPC/OMMT nanocomposites. The excellent gas barrier properties and unique mechanical properties of the nanocomposites prepared in this work have a great potential to broaden the application of sustainable PPC.

Experimental

Materials

PPC, with a number-average molecular weight (M_n) of 77,000 g/mol, was supplied by Tianguan Enterprise (Henan, China). The organo-montmorillonite (trade name was DK2) (OMMT) was kindly provided by Fenghong Clay Co. Ltd., China, modified with methyl tallow bis(2-hydroxyethyl) ammonium.

Preparation of nanocomposites

PPC/clay nanocomposites (PPCCNs) were prepared by direct melt compounding OMMT with PPC in a torque rheometer (XSS-300, Shanghai Kechuang Rubber Plastic Mechanical Equipment Co., Ltd., China) at 150 °C and 90 rpm for 10 min until reach to a constant torque. Six different PPC/OMMT composites with weight ratios of 100/1, 100/2, 100/3, 100/5, 100/7, and 100/10 were prepared. Before melt blending, the PPC pellets were cryogenically pulverized to about 100 μm for 1 min using WJX-A500 mill (Shanghai Yuanwo Industry and Trade Co., Ltd.) to prepare

more homogeneous preblends with OMMT. Then, all the preblends were dried at 40 °C under vacuum for 24 h before using. For better comparison, the pure PPC sample was also processed in rheometer to keep identical thermal history with PPCCNs. After melt mixing, the samples were hot-pressed at 170 °C for 5 min and then cold-pressed at room temperature to form 0.7 and 0.2 mm thick sheets to satisfy the need of different measurement, respectively. In the discussion, the resultant samples were briefly designated as PPCx, with x denoting the weight percentage of OMMT, such as PPC3 is referred as nanocomposite with 3 phr OMMT (phr = parts per hundred parts of PPC).

Characterization

A D8 advance X-ray diffractometer (Bruker, Germany) was used to characterize the X-ray diffraction (XRD) patterns of the samples. The Cu K α radiation ($\lambda = 0.15418$ nm) source was operated at 40 kV and 200 mA. The scanning angle (2θ) covered a range of 1°–10° for PPC/OMMT nanocomposites and neat OMMT at a speed of 3° min⁻¹ at room temperature.

The transmission electron microscope (TEM) measurements were made on a JEM-2010 (HR) high-resolution transmission electron microscope operating at 200 kV. The samples for TEM were sliced up using a cryo-microtome (Leica RM2125, Germany). Ultrathin films of nanocomposites with thickness of 60 nm were adhered onto copper web before observing. The field-emission scanning electron microscope (SEM) (XL30 ESEM FEG, FEI Co., Eindhoven, The Netherlands) was also applied to observe the morphology of nanocomposites. The constant accelerating voltage was set at 10 kV. The specimens for SEM were cryo-fractured after immersing in liquid nitrogen for at least 20 min and the fractured surfaces were sputtering coated with a thin layer of gold under vacuum before the measurement. The magnification used in SEM microscopy for OMMT nanoplatelets is 10,000 and that for other samples is 2000.

The Fourier transform infrared (FTIR) spectra were collected with a Bruker Vertex-70 instrument. The spectra of neat PPC, PPC3, and PPC10 films were collected in the reflection mode; the spectrum of powdery OMMT was collected in transmission mode. The spectra within the range 4000–400 cm⁻¹ with a resolution of 4 cm⁻¹ were recorded.

Thermal analysis was performed using a TA Instruments differential scanning calorimeter DSC Q20 (USA) under N₂ atmosphere. The specimens with a nominal weight of about 7 ± 0.3 mg were sealed in aluminum crucibles. The measured specimens were firstly heated from 20 to 140 °C at a heating rate of 30 °C/min, after erasing the previous thermal history, and then cooled to 0 °C at a rate of 10 °C/min. The samples were further heated to 140 °C again from 0 °C at a heating rate of 10 °C/min.

The thermal stability of materials was measured by thermogravimetric analysis (TGA) on a METTLER STAR. The samples were gradually heated at a rate of 10 °C/min from 50 to 600 °C under the protection of N₂ atmosphere.

Rheological measurements were carried out using a rotational rheometer (TA Series AR2000ex, TA Instrument, USA). The compression-molded samples were

cut into the disks (25 mm in diameter and 0.7 mm in thickness). The measurements were performed in dynamic (oscillatory) mode by means of 25 mm parallel geometry at 150 °C under an air atmosphere. Amplitude sweeps were performed in advance to ensure that the dynamic tests were in the linear viscoelastic range and a strain value of 1.25% was consequently chosen. Dynamic frequency sweep tests were executed in the ranged of 0.1–100 rad/s.

The oxygen permeation rate of the samples was measured according to ISO 2556: 1974 using gas permeation instrument VAC-V2 (labthink instruments, Jinan, China). The measurements were performed using a constant-volume method at a given pressure of 1 atm and a constant temperature of 23 °C (0% RH). Before testing, the specimens were clamped tightly in test chambers. At first, the pure nitrogen entered into the lower half of the chamber and high pure oxygen was introduced in the other half of the chamber. Oxygen molecules were taken to the sensor after permeating the specimen from the upper cavity into the another side. The sensor detected the concentration of the permeable oxygen and transformed them into the gas permeability rate expressed in cm^3/m^2 day. The oxygen permeability coefficient (OP) which was also given by the instrument was calculated from the measured gas permeability rate. The permeability of each specimen was taken an average value of three tests.

Tensile properties were measured using an Instron-1121 tensile tester in accordance with the standard ISO 527-93. The measurement was taken at room temperature with an extension speed of 10 mm/min. The compressed specimens were prepared into a dumbbell type with dimensions of 20 mm (effective length) \times 4 mm (narrow portion width) \times 0.7 mm (thickness). All specimens were stored for over 24 h under the test condition, and an average value of at least five tests was taken for each specimen.

Results and discussion

Dispersion of OMMT in PPC matrix

XRD is an effective method to characterize nanocomposites on the nanostructure level. Figure 1 shows the XRD patterns of PPC/OMMT composites with different clay contents and the corresponding values of 2θ are listed in Table 1. The XRD patterns display that after blending with PPC, the initial diffraction peak (001) of OMMT shifts from $2\theta = 3.9^\circ$ to almost 2.6° . This result is ascribed to the intercalation of PPC macromolecular chains into the layers of silicate, resulting in the interlayer distance of OMMT increased as already observed by Tunc and Duman [26]. The (001) diffraction peaks of PPC/OMMT composites with clay contents from 1 to 10 phr locate at $2\theta = 2.4^\circ$ – 2.7° , indicating that the intercalation of PPC chains increases the d_{001} spacing of OMMT more than 1 nm. Moreover, there is no significant difference which can be discerned inducing by the content of OMMT and the processing procedure. In the case of PPC5, PPC7, and PPC10 composites, there are small peaks appearing at $2\theta = 5.0^\circ$ corresponding to a d -spacing of 1.7 nm. It is believed that the presence of hydroxylated edge–edge interaction of the silicate

Fig. 1 XRD patterns of the samples with different PPC/OMMT ratios via melt intercalation

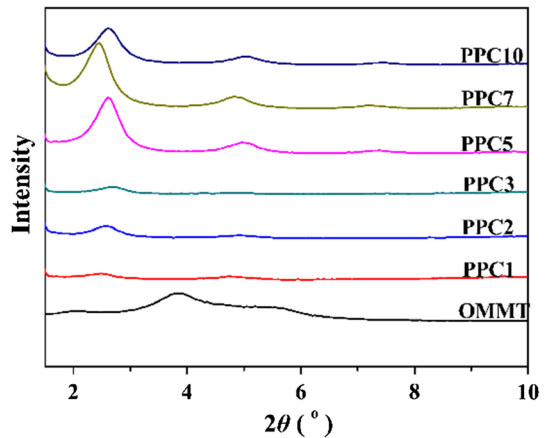


Table 1 Diffraction peaks and interlayer spacing of PPC/OMMT nanocomposites

	2θ (°)	d_{001} (nm)
OMMT	3.9	2.2
PPC1	2.5	3.5
PPC2	2.6	3.4
PPC3	2.7	3.3
PPC5	2.6	3.4
PPC7	2.4	3.6
PPC10	2.6	3.4

layers leads to the flocculation of stacked and intercalated silicate layers [27]. What worth noting is that the intensity of the (001) diffraction peaks with the content of OMMT more than 3 phr is higher evidently than that of composites with lower concentration of clays. Some reports stated that the lower intensity of the peaks was attributed to the partial exfoliation of the OMMT platelets when the concentration of OMMT was not too high [28]. Otherwise, from the aspect of peak intensity, it seems that the agglomeration of clays increases upon increasing clay loadings.

Morphology of PPC/OMMT nanocomposites

Figure 2 presents the TEM images of PPC3 and PPC10 nanocomposites. In these images, part of OMMT nanoplatelets denoted as the dark lump have been intercalated and some individual nanoplatelets disperse homogeneously in PPC matrix with a slice size lower than 1 μm . A minor extent of OMMT reveals a number of agglomerates in PPC3; however, the dispersion of individual silicate layers in the polymer matrix for PPC10 is less homogeneous than PPC3. In Fig. 2c, the magnified sample edge of PPC10 is given to present the morphology of the nanocomposites more clearly. From Fig. 2c, we confirm that the PPC/OMMT nanocomposites are prepared successfully and the nanoplatelets are embedding in the PPC matrix as we think. It also can be seen the distribution of the clays in the

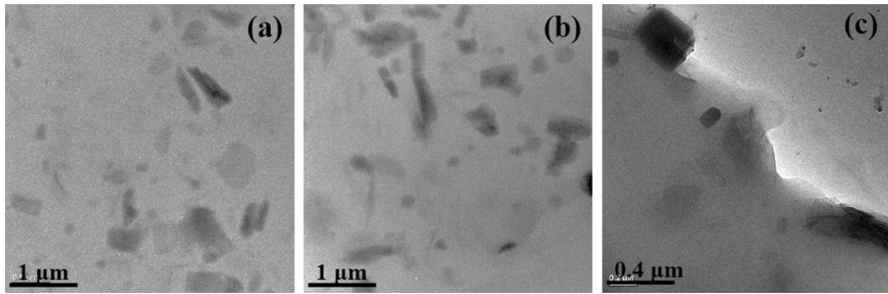


Fig. 2 TEM micrographs of **a** PPC3, **b** PPC10, and **c** the sample edge of PPC10

PPC matrix which depends on the amount of the OMMT which is consist with the result of XRD. Even so, both PPC3 and PPC10 are considered as a partial intercalated system.

The SEM micrograph of pure OMMT is shown in Fig. 3a, while neat PPC and the nanocomposites SEM images are displayed in Fig. 3b–d. The image of OMMT reveals an apparent layered structure and the original stack size of lamellar structure is close to 4–6 μm. From the cross-section images of the PPC/OMMT composites, it can be seen that the surface morphology changes according to the clay loading. For brevity, we just list some representative micrographs. Neat PPC shows a smooth surface, and the evenly dispersed white dots in the PPC matrix are residual Zinc

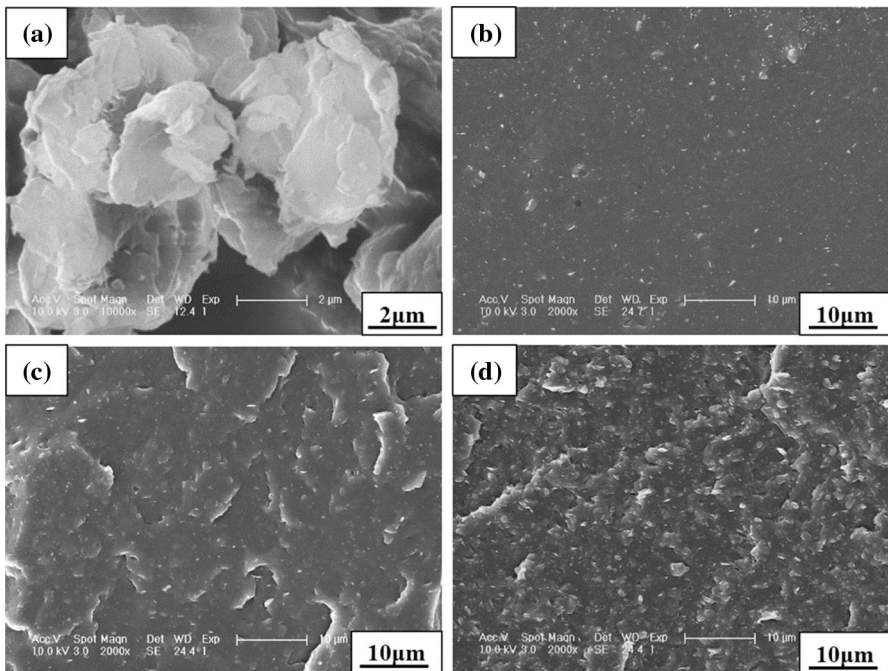


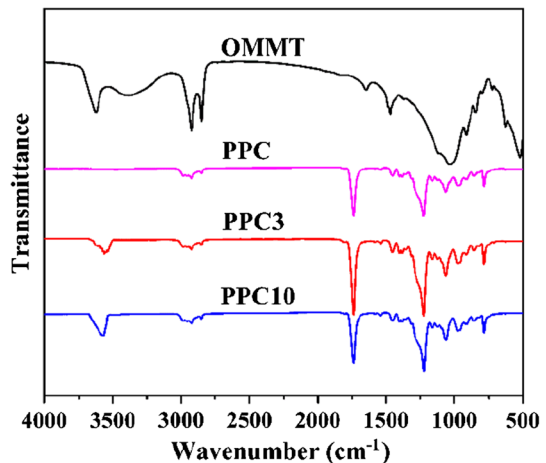
Fig. 3 SEM micrographs: **a** OMMT, **b** neat PPC, **c** PPC3, and **d** PPC10

catalysts which have been verified by EDAX (Energy-dispersive X-ray spectroscopy). Moreover, PPC3 reveals a homogenous dispersion of OMMT in the polymer matrix, though the surface becomes a little rough. The image of PPC10 displays a rougher surface and presents some microscale fillers and gaps due to the agglomeration of individual silicate layers. Both the micrographs and XRD results indicate that the organic modified clays can homogeneously disperse in the polymer matrix at a small amount; however, agglomeration may form with higher loadings of OMMT added.

Interaction between PPC and OMMT

The FTIR spectra of powdery OMMT, neat PPC film, and PPC10 film are illustrated in Fig. 4. In spectrum of OMMT, the peaks at 2915 and 2849 cm^{-1} are assigned to the characteristic absorptions of the C–H stretching vibration of the alkylammonium. The broad band in the region of 3623 cm^{-1} attributes to the stretching vibration of the –OH of the methyl tallow bis(2-hydroxyethyl) ammonium. The FTIR reflection spectra of pure PPC film exhibits some characteristic absorption peaks corresponding to polymeric groups of PPC. That peaks at 2850–3000 cm^{-1} , 1739, 1231, 1062, 784, and 1120 cm^{-1} which confirms the presence of C–H, C=O, C–O, and C–O–C functional groups, respectively. The spectra of the PPC3 and PPC10 nanocomposites show the characteristic peaks of both PPC and OMMT which confirms that the PPC/OMMT nanocomposites are prepared successfully. The nanocomposites exhibit a peak assigned to the hydroxyl stretching of OMMT appeared at 3621 cm^{-1} . The carbonyl band at 1737 cm^{-1} is wider, more intense, and about 2 cm^{-1} lower than that of the neat PPC. Both the shift of hydroxyl peak for neat OMMT and the carbonyl peak for neat PPC indicate the formation of hydrogen bond between the hydroxyl group of OMMT and the carbonyl group of PPC in the nanocomposites [29]. It is worth noting that the peak intensity of PPC3 at 1737 cm^{-1} is higher than that of PPC10, which suggests that the interaction between PPC and OMMT in PPC3 is slightly higher than in PPC10. This result

Fig. 4 FTIR spectra of OMMT, neat PPC, PPC3, and PPC10 composite films



consists with the dispersion of OMMT in the PPC matrix demonstrated former that better dispersion of OMMT results from better PPC-OMMT reaction.

Thermal behaviors

Thermal properties are important characteristics for thermoplastics, as they usually give suggestions for the processing temperature range. In this research, DSC and TGA are performed under nitrogen atmosphere to investigate the influence of the OMMT on the thermal behaviors of the PPC/OMMT nanocomposites films. The thermograms are depicted in Figs. 5 and 6, respectively.

The glass transition temperature (T_g) are investigated by DSC measurement and the relevant values are obtained from the second heating process after erasing the thermal history. The value of T_g increases slightly with the increases of OMMT content, as summarized in Table 2. The behavior that the T_g values of nanocomposites increase with filler content increasing has been stated by other reports [21, 24, 30]. The thermodynamic model, which was proposed by Lee [31] based on the configurational entropy model and the Floy-Huggins theory, describes the variation of T_g in binary polymer/nanofillers system. Both increase and decrease of T_g that would present after the addition of nanocomposites to an amorphous polymer depended on the interaction between the matrix and fillers. In short, the strong interaction between matrix and nanofillers will bring an increment of T_g . On the contrary, T_g decreases in the system with a very low interaction or without any interaction. Consequently, the phenomenon that T_g increases with the augment of the content of OMMT illustrates that there is some interaction between PPC matrix and OMMT particles which is consistent with the result of FTIR.

The thermal stability behaviors of PPC and PPC/OMMT nanocomposites are further studied by TGA measurement. Figure 6a, b shows the thermal gravimetric analysis (TGA) and differential thermal analysis (DTG) of PPC/OMMT nanocomposites with different clay contents. It clearly reveals in Table 2 that the 5 wt% weight loss temperature ($T_{-5\%}$) of PPC3 is almost 19 °C higher than that of pure

Fig. 5 DSC thermograms recorded during second heating scans of PPC/OMMT composites at the rate of 10 °C/min

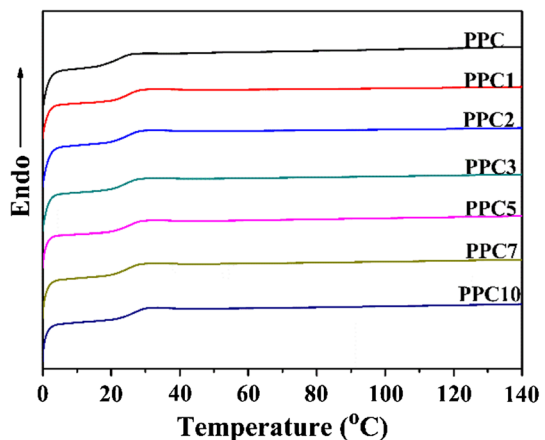


Fig. 6 TGA and DTG curves of the PPC/OMMT composites. The illustration in **a** and **b** is TGA and DTG curves of OMMT, respectively

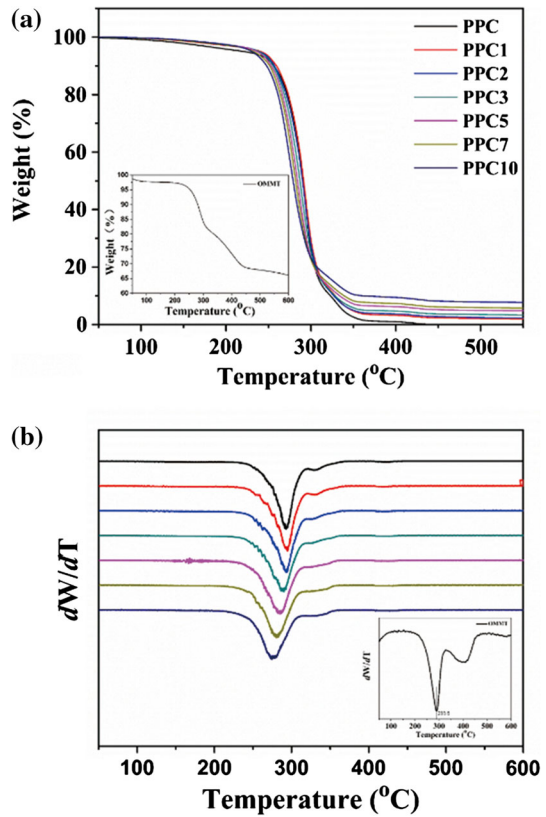


Table 2 Thermal properties of PPC/OMMT nanocomposites

	T_g (°C)	T_d (°C)	$T_{-5\%}$ (°C)	T_{max} (°C)
PPC	22.4	267.1	220.8	334.8
PPC1	24.8	264.8	240.7	293.7
PPC2	24.7	261.4	238.9	292.9
PPC3	24.4	263.8	238.9	288.9
PPC5	24.9	259.4	236.6	285.3
PPC7	24.6	258.7	232.5	280.9
PPC10	26.2	256.9	230.2	275.7

PPC. However, the $T_{-5\%}$ decreases slightly as the content of OMMT continues increasing but still higher than that of pure PPC. The variation tendency of $T_{-5\%}$ is similar to the PPC/OMMT nanocomposites reported by Xu [24]. Moreover, it is also noticeable that the initial decomposition temperature has decreased gradually from 267 °C for neat PPC to 257 °C for PPC10. The maximal decomposition temperature (T_{max}) of PPC10 reflected in DTG graph decreases about 60 °C compared with that of neat PPC. The poor thermal stability of PPC/OMMT composites discovered in our study is contrary to other researches [21, 32, 33], in which they showed that the

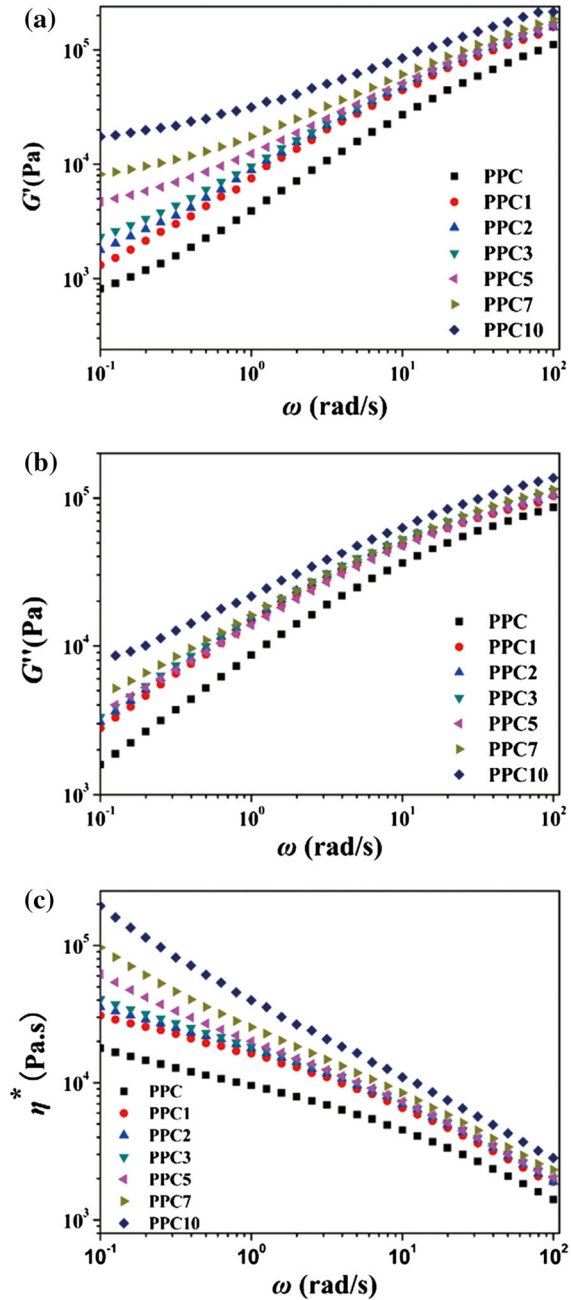
decomposition temperature of PPC/clay nanocomposites had enhanced by almost 50 °C. The phenomenon is on account of the poor thermal stability and high content of organic modifier. From the illustrations in Fig. 7a, b, we find that the content of modifier is 35 wt% of OMMT. In addition, the $T_{-5\%}$ and $T_{-10\%}$ of these organic substances on the surface of OMMT are 253 and 280 °C, respectively. Both the two temperatures are nearly 20 °C lower than those corresponding values of OMMT in other reports [32]. We believe that the increase in $T_{-5\%}$ of composites can be attributed to the dispersed adiabatic silicate layers which form protective barriers on the surface of PPC and impede the heat conduction in the matrix. Otherwise, the polymer macromolecule chains just breakage and a small amount of volatile molecules generate to be detected for the instrument at relatively lower temperature. With temperature elevated, the long molecular chains of PPC are disassembled into short units, because the excess poor thermal stable methyl tallow bis(2-hydroxyethyl) ammonium groups on the layer surface of OMMT accelerate the thermal degradation of PPC, leading to the T_{\max} decrease for all nanocomposites [25]. In addition, there are no residues for neat PPC with temperature elevated to 450 °C. However, the residues content for all nanocomposites increases with the increase content of OMMT. This is due to the residues which are inorganic MMT platelets which are not thermal degradable. According to the variation trend of $T_{-5\%}$, it confirms that the thermal properties of nanocomposites are strongly dependent on the dispersion of nanofillers.

Rheological properties

PPC/OMMT nanocomposites exhibit different rheological behaviors as compared with neat PPC. Figure 7 shows the rheological properties represented by curves of $\log G'$, $\log G''$, and $\log \eta^*$ as a function of $\log \omega$ for the considered samples. One can see that the higher organoclay concentration, the larger increment of G' and G'' , especially at lower frequency, caused by the reinforcement of the fillers. The reinforcing effect results from the hydrogen bonding interactions between the hydroxyl groups in the organic modifier of the OMMT and the carbonyl group of PPC chain segments [21]. It is notable that at higher frequencies, the values of G' and G'' are both comparable for all the samples, and this declares that at higher frequencies, the response of the samples is mainly determined by the properties of the polymer matrix and has little relation to the content of OMMT [34].

We also compare the variation trend of the storage modulus and loss modulus with the change of frequency for all the samples, as exhibited in Fig. 8. For the molten nanocomposites with less content of OMMT and neat PPC, they reveal a classical liquid-like behavior at lower frequency, that G' is smaller than G'' . The difference between G' and G'' decreases gradually with raising deformation frequency and then G' is larger than G'' at the highest ω , behaving as an elastic polymer. Moreover, for PPC5, two crossover points are observed: $\omega_1 = 0.35$ and $\omega_2 = 5.41$ rad/s. Between ω_1 and ω_2 , the behavior of the samples is liquid-like ($G' < G''$). Below ω_1 , G' exceeds G'' which indicates the so-called “pseudo-solid-like behavior” of the material at low deformation frequencies. For the nanocomposites PPC7 and PPC10, they behave as pseudo-solid-like polymers that G'

Fig. 7 Comparison of rheological properties of PPC/OMMT: **a** storage modulus, **b** loss modulus, and **c** complex viscosity



exceeds G'' at all the range of ω . As can be seen, the rheological properties of nanocomposites have changed from liquid-like response to solid-like response, which is ascribed to the formation of the threshold network of the PPC/OMMT nanocomposites with the gradual addition of OMMT.

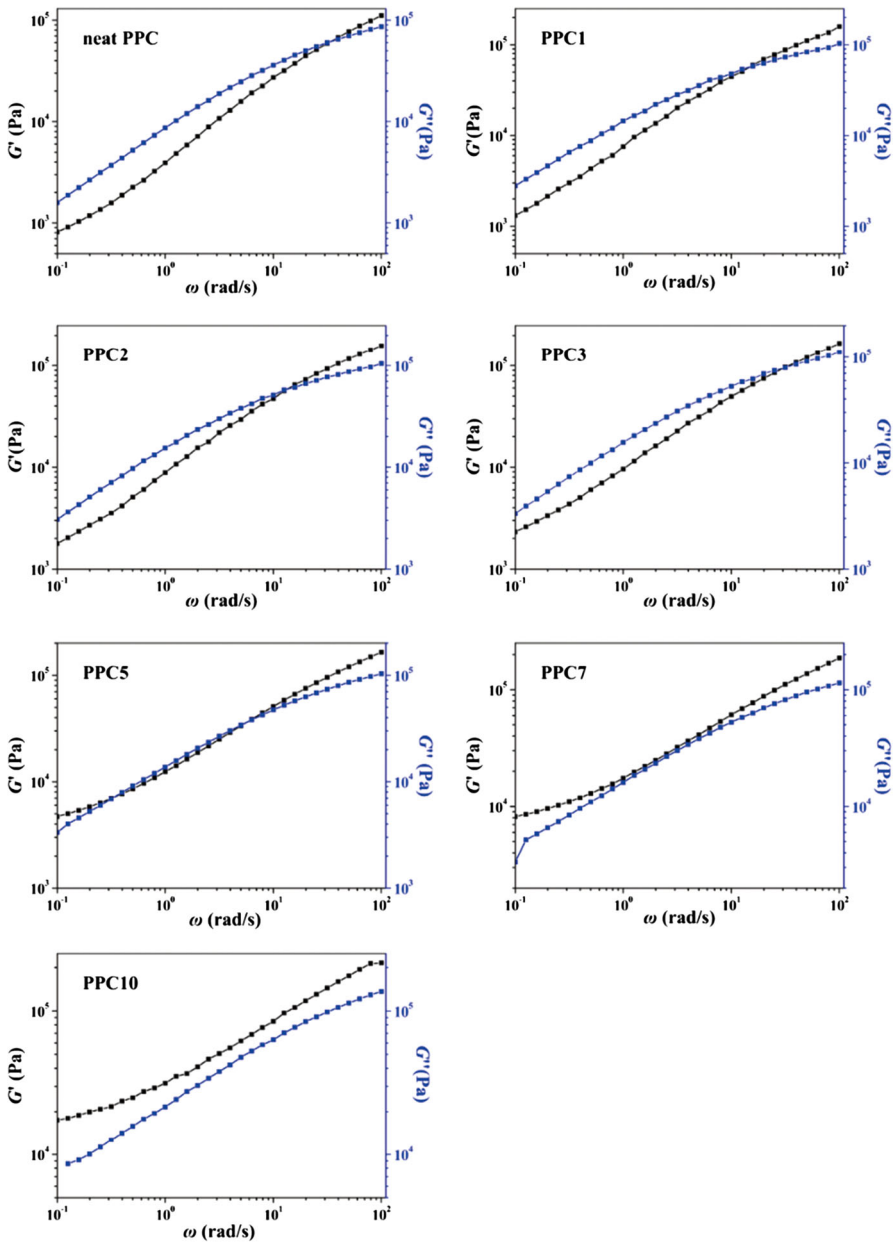


Fig. 8 Frequency dependencies of the storage modulus (G') and loss modulus (G'') of neat PPC and PPC/OMMT composites

Mechanical properties

The mechanical properties of PPC/OMMT nanocomposites are shown in Fig. 9. As list in Table 3, it reveals that the yield strength and modulus increase stepwise with the increase of OMMT content up to 3 phr, which suggests that the high aspect ratio platelets OMMT reinforce the PPC matrix. Usually, the incorporation of clays into polymer matrix usually decreases the elongation of composites significantly. In the report of PPC/organo-vermiculite(VMT) nanocomposites put forward by Xu [25], the elongation at break of nanocomposites decreased from 17.6% of pure PPC to 7.6% of PPC/4%VMT. In addition, the incorporation of 3 wt% of OMMT in PLA/clay nanocomposites also made the elongation at break of neat PLA decrease from 29.0 to 7.8% [35]. However, in our PPC/OMMT nanocomposites, the elongation at break increases upon increasing the content of OMMT, and the optimal elongation is observed at 3 phr OMMT with a value of 538.1%, suggesting an excellent toughness of the composites. Tensile fracture energy (E_{TF}) shows the energy absorbed before tensile fracture, which is another important characterization of material tensile toughness. E_{TF} is defined as area enclosed by stress–strain curve from tensile fracture and calculates according to trapezoid rules [36]. The values of E_{TF} increase sharply and then decrease slightly

Fig. 9 Stress–strain curves of neat PPC and PPC/OMMT composites

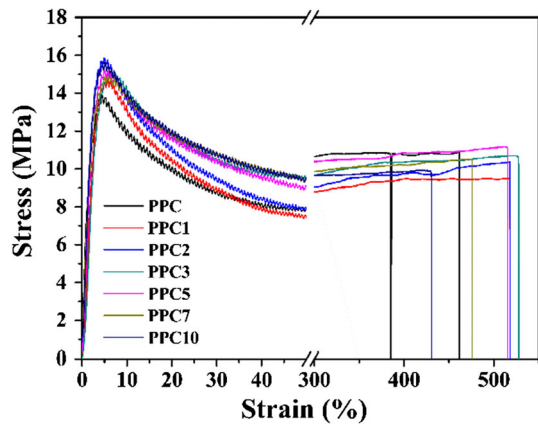


Table 3 Mechanical properties of neat PPC and PPC/OMMT blends

	Modulus (MPa)	Yield strength (MPa)	Elongation at break (%)	E_{TF} (J)
PPC	551.3 ± 15.2	12.2 ± 1.2	361.9 ± 32.7	2.71 ± 0.12
PPC1	525.7 ± 11.1	14.7 ± 1.3	517.6 ± 24.2	3.16 ± 0.06
PPC2	653.7 ± 35.2	15.9 ± 0.2	521.6 ± 5.2	3.39 ± 0.09
PPC3	741.6 ± 19.2	16.7 ± 1.0	538.1 ± 15.5	3.46 ± 0.10
PPC5	554.8 ± 24.1	14.4 ± 0.1	521.5 ± 8.6	3.31 ± 0.06
PPC7	646.2 ± 22.3	14.5 ± 0.6	464.2 ± 16.5	3.24 ± 0.11
PPC10	736.7 ± 15.6	15.6 ± 1.4	356.2 ± 18.0	2.97 ± 0.03

with the further increment of OMMT, which manifest that the addition of OMMT is beneficial to improving tensile toughness of the composites.

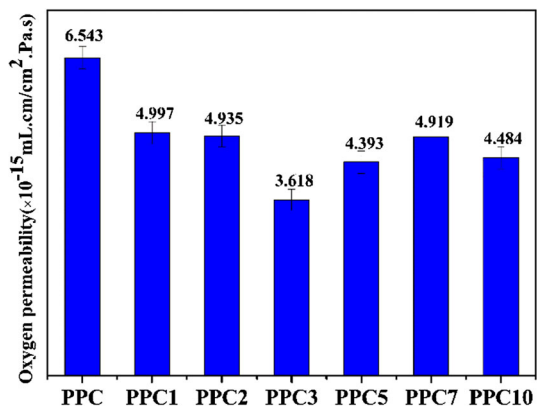
From the variation of tensile strength, modulus, elongation at break, and the value of E_{TF} with the incorporation of OMMT, we find that the composite with 3 phr OMMT has the optimal tensile performance. It is believed that the superior mechanical properties are associated with the well dispersion of OMMT in polymer matrix, because the dispersed nanofillers make the stress transfer from polymer matrix to the platelets of OMMT [37].

Gas barrier properties

Good gas barrier materials can reduce the oxygen permeability rate so as to prolong the shelf life of products. Lamellar inorganic fillers are considered as impenetrable by gas molecules, and thus, the incorporation of OMMT can lengthen tortuosity route for gas molecules transporting and retard the penetration process so as to improve barrier properties of the composites. The processing method of polymer/clay nanocomposites can play a key role in the distribution of the nanoplatelets in the matrix and, therefore, determines the barrier characteristics of the resulting materials. The melt intercalation technique has widely been used to make polymer/clay nanocomposites because of convenient processing. In the process of melt compounding, the imposed external shear force makes the layered clays be intercalated and disperse in the molten polymer matrix.

In this study, values of oxygen permeability coefficient (OP) of the PPC/OMMT nanocomposites are shown in Fig. 10 to evaluate the oxygen barrier properties of the composites. It is obvious that the OP decreases stepwise with the content of OMMT up to 3 phr and then increases slowly with more OMMT added. The OP of the PPC3 reduces by 44.7% of pure PPC. It is well known that the gas barrier properties of nanocomposites are mainly determined by the morphology and dispersion of clay nanoplatelets in polymers. This can be attributed to the well-dispersed platelets lengthen a bypass path of gas molecules effectively. The value of OP increases slowly when continue adding OMMT indicates that the oxygen barrier

Fig. 10 Oxygen permeability of neat PPC and PPC/OMMT composites



properties of the composites reduce with excess OMMT. It may be that the aggregation of OMMT leads to the emergence of gaps between the interface of matrix and OMMT particles, as shown in Fig. 3d, which makes the gas molecules to pass through polymer films easily. Free volume is considered as a channel for gas molecules transporting through the polymer membrane, which is caused by chain packing and chain segment rearrangement. Wilson et al. [38] used positron annihilation lifetime spectroscopy (PALS) technique to study the free volume changes in the EVA/OMMT composites. They found that the relative fractional free volume decreased in homogeneous composites attributed to the interaction between high aspect ratio of platelet layered silicates and polymer. However, the excess fillers began aggregate, additional voids were introduced and caused the free volume increase, leading to the permeation of gas easier. Our research is similar to the previous reports that the gas permeability decreases in well-dispersed nanocomposites. Generally speaking, the homogeneous composites can bring superior oxygen barrier properties and may contribute to broadening the wide range application of PPC in packing industry.

Conclusions

PPC/OMMT nanocomposites with different concentration of OMMT were fabricated by a facilitate and effective melt blending method. The results of XRD, TEM, and SEM indicated that OMMT could well disperse in the PPC matrix and were intercalated by PPC macromolecules. The addition of organic modified OMMT made an increase in the T_g of PPC due to the interaction between matrix and nanoparticles demonstrated by FTIR spectra. According to the results of TGA, $T_{-5\%}$ of the composites increased because of the protective function of these adiabatic silicate layers. However, the initial thermal decomposition temperature of PPC decreased, since the high content of organic modifier accelerated the thermal degradation of PPC at elevated temperature. The formation of percolation network made the rheological properties of PPC/OMMT nanocomposites translated from a liquid-like behavior to a solid-like one, after the incorporation of sufficient OMMT. Interestingly, PPC/OMMT nanocomposites possessed not only higher modulus and strength; the toughness of the composites was enhanced simultaneously. The oxygen permeability of well-dispersed PPC/OMMT nanocomposite with 3 phr OMMT reduced by 44.7% compared with that of pure PPC. The superior oxygen barrier properties and preferable mechanical properties of PPC/OMMT nanocomposites consequently expanded the application fields of PPC.

Acknowledgements This work is supported by the Government of Taian city and Science and Technology Department of Shandong Province (2015ZDZX11002). Part of this work is supported by program of Cooperation of Hubei Province and Chinese Academy of Sciences, Jilin Province Science and Technology Agency (20160204030GX), and program of Changchun Municipal Scientific and Technologic Development (16SS16).

References

1. Cui Y, Kumar S, Rao Kona B, van Houcke D (2015) Gas barrier properties of polymer/clay nanocomposites. *RSC Adv* 5(78):63669–63690. doi:[10.1039/c5ra10333a](https://doi.org/10.1039/c5ra10333a)
2. Inoue SKH, Tsuruta T (1969) Copolymerization of carbon dioxide and epoxide. *J Polym Sci Part B Polym Lett* 7:287–292
3. Chen S, Chen B, Fan J, Feng J (2015) Exploring the application of sustainable poly(propylene carbonate) copolymer in toughening epoxy thermosets. *ACS Sustain Chem Eng* 3(9):2077–2083. doi:[10.1021/acssuschemeng.5b00343](https://doi.org/10.1021/acssuschemeng.5b00343)
4. Barreto C, Hansen E, Fredriksen S (2012) Novel solventless purification of poly(propylene carbonate): tailoring the composition and thermal properties of PPC. *Polym Degrad Stab* 97(6):893–904. doi:[10.1016/j.polymdegradstab.2012.03.033](https://doi.org/10.1016/j.polymdegradstab.2012.03.033)
5. Yao M (2011) Modification of poly(lactic acid)/poly(propylene carbonate) blends through melt compounding with maleic anhydride. *Express Polym Lett* 5(11):937–949. doi:[10.3144/expresspolymlett.2011.92](https://doi.org/10.3144/expresspolymlett.2011.92)
6. J-y Park, Lee E-S, Amna T, Jang Y, Park DH, Kim B-S (2016) Effects of heat-treatment on surface morphologies, mechanical properties of nanofibrous poly(propylene carbonate) biocomposites and its cell culture. *Colloids Surf A* 492:138–143. doi:[10.1016/j.colsurfa.2015.11.075](https://doi.org/10.1016/j.colsurfa.2015.11.075)
7. Hwang SW, Park DH, Kang DH, Lee SB, Shim JK (2016) Reactive compatibilization of poly(L-lactic acid)/poly(propylene carbonate) blends: thermal, thermomechanical, and morphological properties. *J Appl Polym Sci* 133 (18):1–10. doi:[10.1002/app.43388](https://doi.org/10.1002/app.43388)
8. Manavitehrani I, Fathi A, Wang Y, Maitz PK, Dehghani F (2015) Reinforced Poly(Propylene Carbonate) Composite with Enhanced and Tunable Characteristics, an Alternative for Poly(lactic Acid). *ACS Appl Mater Interfaces* 7(40):22421–22430. doi:[10.1021/acsami.5b06407](https://doi.org/10.1021/acsami.5b06407)
9. Yang G, Hu X, Su J, Geng C, Yao W, zhang Q, Fu Q (2013) Significant reinforcement of poly(propylene carbonate): nanostructured polymer composites of poly(propylene carbonate)/poly(methyl methacrylate) via a supercritical carbon dioxide route. *J Supercrit Fluids* 82:200–205. doi:[10.1016/j.supflu.2013.08.003](https://doi.org/10.1016/j.supflu.2013.08.003)
10. Giannelis EP (1996) Polymer layered silicate nanocomposites. *Adv Mater* 8(1):29–35. doi:[10.1002/adma.19960080104](https://doi.org/10.1002/adma.19960080104)
11. Giannelis EP, Krishnamoorti R, Manias E (1999) Polymer-silicate nanocomposites: model systems for confined polymers and polymer brushes. *Polym Confin Environ* 138:107–147
12. Kiliaris P, Papispyrides CD (2010) Polymer/layered silicate (clay) nanocomposites: an overview of flame retardancy. *Prog Polym Sci* 35(7):902–958. doi:[10.1016/j.progpolymsci.2010.03.001](https://doi.org/10.1016/j.progpolymsci.2010.03.001)
13. LeBaron PC, Wang Z, Pinnavaia TJ (1999) Polymer-layered silicate nanocomposites: an overview. *Appl Clay Sci* 15(1–2):11–29. doi:[10.1016/s0169-1317\(99\)00017-4](https://doi.org/10.1016/s0169-1317(99)00017-4)
14. Choudalakis G, Gotsis AD (2009) Permeability of polymer/clay nanocomposites: a review. *Eur Polym J* 45(4):967–984. doi:[10.1016/j.eurpolymj.2009.01.027](https://doi.org/10.1016/j.eurpolymj.2009.01.027)
15. Du A, Genero A, Koo D, Sundararaj U, Cairncross R (2012) Water transport in polylactide and poly(lactide)/montmorillonite composites. *J Polym Environ* 21(1):8–15. doi:[10.1007/s10924-012-0540-4](https://doi.org/10.1007/s10924-012-0540-4)
16. Żenkiewicz M, Richert J (2008) Permeability of polylactide nanocomposite films for water vapour, oxygen and carbon dioxide. *Polym Test* 27(7):835–840. doi:[10.1016/j.polymertesting.2008.06.005](https://doi.org/10.1016/j.polymertesting.2008.06.005)
17. Kawasumi M (2004) The discovery of polymer-clay hybrids. *J Polym Sci Polym Chem* 42(4):819–824. doi:[10.1002/pola.10961](https://doi.org/10.1002/pola.10961)
18. Kojima Y, Usuki A, Kawasumi M, Okada A, Kurauchi T, Kamigaito O (1993) Synthesis of nylon-6-clay hybrid by montmorillonite intercalated with epsilon-caprolactam. *J Polym Sci Polym Chem* 31(4):983–986. doi:[10.1002/pola.1993.080310418](https://doi.org/10.1002/pola.1993.080310418)
19. Kojima Y, Usuki A, Kawasumi M, Okada A, Kurauchi T, Kamigaito O (1993) One-pot synthesis of nylon-6 clay hybrid. *J Polym Sci Polym Chem* 31(7):1755–1758. doi:[10.1002/pola.1993.080310714](https://doi.org/10.1002/pola.1993.080310714)
20. Ray SS, Okamoto M (2003) Polymer/layered silicate nanocomposites: a review from preparation to processing. *Prog Polym Sci* 28(11):1539–1641. doi:[10.1016/j.progpolymsci.2003.08.002](https://doi.org/10.1016/j.progpolymsci.2003.08.002)
21. Shi X, Gan Z (2007) Preparation and characterization of poly(propylene carbonate)/montmorillonite nanocomposites by solution intercalation. *Eur Polym J* 43(12):4852–4858. doi:[10.1016/j.eurpolymj.2007.09.024](https://doi.org/10.1016/j.eurpolymj.2007.09.024)

22. Takahashi S, Goldberg HA, Feeney CA, Karim DP, Farrell M, O'Leary K, Paul DR (2006) Gas barrier properties of butyl rubber/vermiculite nanocomposite coatings. *Polymer* 47(9):3083–3093. doi:[10.1016/j.polymer.2006.02.077](https://doi.org/10.1016/j.polymer.2006.02.077)
23. Khan SB, Akhtar K, Seo J, Han H, Rub MA (2012) Effect of nano-filler dispersion on the thermal, mechanical and water sorption properties of green environmental polymer. *Chinese J Polym Sci* 30(5):735–743. doi:[10.1007/s10118-012-1168-5](https://doi.org/10.1007/s10118-012-1168-5)
24. Xu J, Li RKY, Meng YZ, Mai YW (2006) Biodegradable poly(propylene carbonate)/montmorillonite nanocomposites prepared by direct melt intercalation. *Mater Res Bull* 41(2):244–252. doi:[10.1016/j.materresbull.2005.08.019](https://doi.org/10.1016/j.materresbull.2005.08.019)
25. Xu J, Li RKY, Xu Y, Li L, Meng YZ (2005) Preparation of poly(propylene carbonate)/organo-vermiculite nanocomposites via direct melt intercalation. *Eur Polym J* 41(4):881–888. doi:[10.1016/j.eurpolymj.2004.10.033](https://doi.org/10.1016/j.eurpolymj.2004.10.033)
26. Tunc S, Duman O (2010) Preparation and characterization of biodegradable methyl cellulose/montmorillonite nanocomposite films. *Appl Clay Sci* 48:414–424. doi:[10.1016/j.clay.2010.01.016](https://doi.org/10.1016/j.clay.2010.01.016)
27. Chen B, Evans JRG (2006) Poly(ϵ -caprolactone)—clay nanocomposites structure and mechanical properties. *Macromolecules* 39:747–754
28. Chen G-X (2005) Role of epoxy groups on clay surface in the improvement of morphology of poly(L-lactide)-clay composites. *Macromolecules* 38:3738–3744
29. Diez-Pascual AM, Diez-Vicente AL (2014) Poly(3-hydroxybutyrate)/ZnO bionanocomposites with improved mechanical, barrier and antibacterial properties. *Int J Mol Sci* 15(6):10950–10973. doi:[10.3390/ijms150610950](https://doi.org/10.3390/ijms150610950)
30. Lee Y, Kim D, Seo J, Han H, Khan SB (2013) Preparation and characterization of poly(propylene carbonate)/exfoliated graphite nanocomposite films with improved thermal stability, mechanical properties and barrier properties. *Polym Int* 62(9):1386–1394. doi:[10.1002/pi.4434](https://doi.org/10.1002/pi.4434)
31. Lee KJ, Lee DK, Kim YW, Choe W-S, Kim JH (2007) Theoretical consideration on the glass transition behavior of polymer nanocomposites. *J Polym Sci Part B Polym Phys* 45(16):2232–2238. doi:[10.1002/polb.21178](https://doi.org/10.1002/polb.21178)
32. Zhang Z, Lee J-H, Lee S-H, Heo S-B, Pittman CU (2008) Morphology, thermal stability and rheology of poly(propylene carbonate)/organoclay nanocomposites with different pillaring agents. *Polymer* 49(12):2947–2956. doi:[10.1016/j.polymer.2008.04.034](https://doi.org/10.1016/j.polymer.2008.04.034)
33. Qinghai Z, Fengxiang G, Huimin L, Xianhong W, Xiaojiang Z, Fosong W (2008) Thermal and mechanical properties of Poly(propylene carbonate) nanocomposites with various organo-modified montmorillonites. *Acta Polym Sinica* 1(12):1123–1128. doi:[10.3724/SP.J.1105.2008.01123](https://doi.org/10.3724/SP.J.1105.2008.01123)
34. Pluta M, Jeszka JK, Boiteux G (2007) Polylactide/montmorillonite nanocomposites: structure, dielectric, viscoelastic and thermal properties. *Eur Polym J* 43(7):2819–2835. doi:[10.1016/j.eurpolymj.2007.04.009](https://doi.org/10.1016/j.eurpolymj.2007.04.009)
35. Piekarska K, Sowinski P, Piorkowska E, Haque MMU, Pracella M (2016) Structure and properties of hybrid PLA nanocomposites with inorganic nanofillers and cellulose fibers. *Compos A* 82:34–41. doi:[10.1016/j.compositesa.2015.11.019](https://doi.org/10.1016/j.compositesa.2015.11.019)
36. Xu Y-Q, Qu J-P (2009) Mechanical and rheological properties of epoxidized soybean oil plasticized poly(lactic acid). *J Appl Polym Sci* 112(6):3185–3191. doi:[10.1002/app.29797](https://doi.org/10.1002/app.29797)
37. Thellen C, Orroth C, Froio D, Ziegler D, Lucciarini J, Farrell R, D'Souza NA, Ratto JA (2005) Influence of montmorillonite layered silicate on plasticized poly(L-lactide) blown films. *Polymer* 46(25):11716–11727. doi:[10.1016/j.polymer.2005.09.057](https://doi.org/10.1016/j.polymer.2005.09.057)
38. Wilson R, Plivelic TS, Aprem AS, Ranganathaiah C, Kumar SA, Thomas S (2012) Preparation and characterization of EVA/clay nanocomposites with improved barrier performance. *J Appl Polym Sci* 123(6):3806–3818. doi:[10.1002/app.34966](https://doi.org/10.1002/app.34966)